ULTRADEEP INFRARED ARRAY CAMERA OBSERVATIONS OF SUB-L^* $z \sim 7$ AND $z \sim 8$ GALAXIES IN THE HUBBLE ULTRA DEEP FIELD: THE CONTRIBUTION OF LOW-LUMINOSITY GALAXIES TO THE STELLAR MASS DENSITY AND REIONIZATION

2010 ApJ 708 L26

(http://iopscience.iop.org/2041-8205/708/1/L26)

The Astrophysical Journal, 708:L26–L31, 2010 January 1 doi:10.1088/2041-8205/708/1/L26

ULTRADEEP INFRARED ARRAY CAMERA OBSERVATIONS OF SUB-L^* $z \sim 7$ AND $z \sim 8$ GALAXIES IN THE HUBBLE ULTRA DEEP FIELD: THE CONTRIBUTION OF LOW-LUMINOSITY GALAXIES TO THE STELLAR MASS DENSITY AND REIONIZATION*

I. Labbé[1,9], V. González[2], R. J. Bouwens[2,3], G. D. Illingworth[2], P. A. Oesch[4], P. G. van Dokkum[5], C. M. Carollo[4], M. Franx[3], M. Stiavelli[6], M. Trenti[7], D. Magee[2], and M. Kriek[8]
[1] Carnegie Observatories, Pasadena, CA 91101, USA; ivo@obs.carnegiescience.edu
[2] UCO/Lick Observatory, University of California, Santa Cruz, CA 95064, USA
[3] Leiden Observatory, Leiden University, NL-2300 RA Leiden, The Netherlands
[4] Institute for Astronomy, ETH Zurich, 8092 Zurich, Switzerland; poesch@phys.ethz.ch
[5] Department of Astronomy, Yale University, New Haven, CT 06520, USA
[6] Space Telescope Science Institute, Baltimore, MD 21218, USA
[7] University of Colorado, Center for Astrophysics and Space Astronomy, 389-UCB, Boulder, CO 80309, USA
[8] Department of Astrophysical Sciences, Princeton University, Princeton, NJ 08544, USA
Received 2009 October 8; accepted 2009 November 25; published 2009 December 14

ABSTRACT

We study the *Spitzer* Infrared Array Camera (IRAC) mid-infrared (rest-frame optical) fluxes of 14 newly WFC3/IR-detected $z \sim 7$ z_{850}-dropout galaxies and $5z \sim 8$ Y_{105}-dropout galaxies. The WFC3/IR depth and spatial resolution allow accurate removal of contaminating foreground light, enabling reliable flux measurements at 3.6 μm and 4.5 μm. None of the galaxies are detected to [3.6] $\approx$ 26.9 (AB, 2σ), but a stacking analysis reveals a robust detection for the z_{850}-dropouts and an upper limit for the Y_{105}-dropouts. We construct average broadband spectral energy distributions using the stacked Advanced Camera for Surveys (ACS), WFC3, and IRAC fluxes and fit stellar population synthesis models to derive mean redshifts, stellar masses, and ages. For the z_{850}-dropouts, we find $z = 6.9^{+0.1}_{-0.1}$, $(U-V)_{\rm rest} \approx 0.4$, reddening $A_V = 0$, stellar mass $\langle M^* \rangle = 1.2^{+0.3}_{-0.6} \times 10^9\ M_\odot$ (Salpeter initial mass function). The best-fit ages ~300 Myr, $M/L_V \approx 0.2$, and SSFR ~ 1.7 Gyr^{-1} are similar to values reported for luminous $z \sim 7$ galaxies, indicating the galaxies are smaller but not much younger. The sub-L^* galaxies observed here contribute significantly to the stellar mass density and under favorable conditions may have provided enough photons for sustained reionization at $7 < z < 11$. In contrast, the $z = 8.3^{+0.1}_{-0.2}$ Y_{105}-dropouts have stellar masses that are uncertain by 1.5 dex due to the near-complete reliance on far-UV data. Adopting the 2σ upper limit on the $M/L(z = 8)$, the stellar mass density to $M_{{\rm UV},AB} < -18$ declines from $\rho^*(z = 7) = 3.7^{+1.4}_{-1.8} \times 10^6\ M_\odot$ Mpc^{-3} to $\rho^*(z = 8) < 8 \times 10^5\ M_\odot$ Mpc^{-3}, following $\propto (1+z)^{-6}$ over $3 < z < 8$. Lower masses at $z = 8$ would signify more dramatic evolution, which can be established with deeper IRAC observations, long before the arrival of the *James Webb Space Telescope*.

Key words: galaxies: evolution – galaxies: high-redshift

Online-only material: color figures

1. INTRODUCTION

The reionization epoch represents the latest observational frontier of galaxy formation. Little is known about the galaxy properties during this time, including feedback, metal production, and their contribution to reionization. Extensive studies have been done of galaxies selected by the dropout technique out to $z = 6$ (see, e.g., Stanway et al. 2003; Yan et al. 2004; Bouwens et al. 2006; McLure et al. 2009a). Pushing these studies to $z \gtrsim 7$ has proven extraordinarily challenging: only ~25 high-quality candidates are currently known (Bouwens et al. 2008; Oesch et al. 2009a; Castellano et al. 2009; Ouchi et al. 2009, R. J. Bouwens et al. 2010, in preparation).

The arrival of WFC3/IR aboard the *Hubble Space Telescope* (*HST*) heralds a dramatic improvement in our ability to survey the reionization era, allowing us to identify the predominant low-luminosity galaxies at $z \gtrsim 7$ by their redshifted UV light. Whereas *HST* remains crucial for identifying the galaxies, longer-wavelength data are necessary for constraining the stellar masses and ages. Access to the rest-frame optical is offered by the Infrared Array Camera (IRAC; Fazio et al. 2004) on *Spitzer*, which by itself has permitted estimates of stellar masses for large numbers of $z \sim 5$–6 sources (Eyles et al. 2005; Yan et al. 2006; Stark et al. 2009), and even a few at $z \sim 7$ (Egami et al. 2005; Labbé et al. 2006). One surprising early finding was the number of quite massive $\sim 10^{10}\ M_\odot$ galaxies with appreciable ages (200–300 Myr) suggesting the galaxies formed substantial amounts of stars at even earlier times, well into the epoch of reionization (Stark et al. 2007; Yan et al. 2006).

In this Letter, we extend the stellar mass and age estimates to lower luminosities ($0.06\ L^*_{z=3}$) and higher redshift $z \approx 8$ by analyzing the IRAC mid-IR fluxes of the robust z_{850}-dropout and Y_{105}-dropout galaxy samples found by Oesch et al. (2009b) and Bouwens et al. (2009a) in the newly acquired WFC3/IR data (GO-11563, PI: Illingworth) over the Hubble Ultra Deep Field (HUDF; see also Bunker et al. 2009; McLure et al. 2009b). We adopt an $\Omega_M = 0.3, \Omega_\Lambda = 0.7$, cosmology with

* Based on observations made with the NASA/ESA *Hubble Space Telescope*, which is operated by the Association of Universities for Research in Astronomy, Inc., under NASA contract NAS 5-26555. These observations are associated with programs #11563, 9797. Based on observations with the *Spitzer Space Telescope*, which is operated by the Jet Propulsion Laboratory, California Institute of Technology under NASA contract 1407. Support for this work was provided by NASA through contract 125790 issued by JPL/Caltech. Based on service mode observations collected at the European Southern Observatory, Paranal, Chile (ESO Program 073.A-0764A). Based on data gathered with the 6.5 m *Magellan Telescopes* located at Las Campanas Observatory, Chile.
[9] Hubble Fellow.

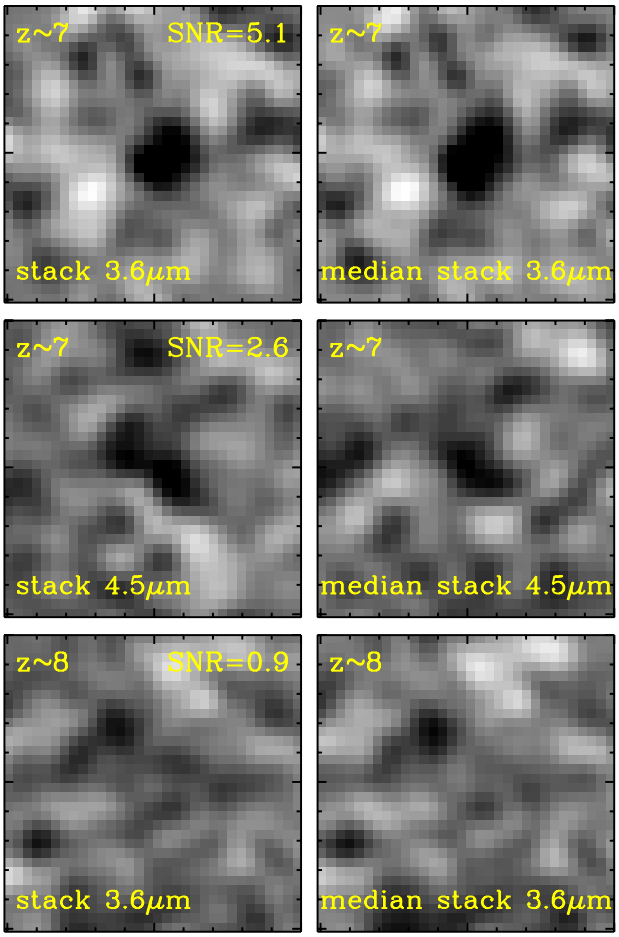

Figure 1. Stacked images of $z \sim 7$ z_{850}-dropout and $z \sim 8$ Y_{105}-dropout sources in the HUDF. The stacked z_{850}-dropouts in the [3.6]-band (top left) shows an unambiguous detection (S/N = 5.1). The median stack also shows a strong signal, indicating that it is not dominated by outliers. The S/N is calculated by bootstrap resampling. The z_{850}-dropouts stack is marginally detected (S/N = 2.6) in [4.5] (middle row). The Y_{105}-dropouts stack (bottom row) shows no source in the center. Panels are in inverted grayscale and $9\farcs9 \times 9\farcs9$ on a side.

(A color version of this figure is available in the online journal.)

$H_0 = 70$ km s^{-1} Mpc^{-1}. Magnitudes are in the AB photometric system (Oke & Gunn 1983). Imaging depths refer to 1σ AB point source total magnitude, unless stated otherwise.

2. OBSERVATIONS AND PHOTOMETRY

The recent $z = 7$ z_{850}-dropout and $z = 8$ Y_{105}-dropout samples were selected from exceptionally deep WFC3/IR imaging, to ≈29 AB magnitude 5σ in Y_{105}, J_{125}, H_{160}, allowing the study of fainter sources than the NICMOS-based samples presented in Labbé et al. (2006) and Gonzalez et al. (2009). We briefly discuss the IRAC photometry of 14 of the 16 z_{850}-dropouts found by Oesch et al. (2009b) and the 5 Y_{105}-dropouts reported by Bouwens et al. (2009a) (see Labbé et al. 2006 for the two z_{850}-dropouts found earlier with NICMOS).

Spitzer data over this field were obtained from the Great Observatories Origins Deep Survey (GOODS; M. Dickinson et al. 2010, in preparation), which observed the HUDF with IRAC in two epochs of ≈23.3 hr each.[10] The IRAC depths in the 3.6 and 4.5 μm bands are 27.7 and 27.2 (AB). We supplement the observations with deep K_s-band data from the Very Large Telescope and *Magellan* to $K_{s,AB} = 27.4$ (I. Labbé et al. 2010, in preparation).

A critical aspect is obtaining reliable IRAC fluxes of the candidates. This is challenging because of the extended wings of the IRAC point-spread function (PSF), causing flux contamination from nearby foreground sources. We use the technique of Labbé et al. (2006) to fit and subtract the foreground sources using the flux profiles in the ultradeep WFC3/IR detection images as priors (see Gonzalez et al. 2009 for a more complete description and Wuyts et al. 2007 for illustrative examples).

After cleaning the IRAC images, we first performed conventional aperture photometry in 3.6 and 4.5 μm bands in $2\farcs5$ diameter apertures. We define the photometric error as the quadratic sum of random fluctuations in the aperture (determined from empty apertures on the nearby background; e.g., Labbé et al. 2003) and the fit uncertainties to each individual neighbor. We performed the photometry independently on the first and second epoch IRAC data, which are rotated by 180 deg and therefore have different PSFs and contamination (see Labbé et al. 2006). Two of the 14 z_{850}-dropouts and 1 Y_{105}-dropout were too close to bright sources to be successfully measured and were removed from the sample (later we assume average M/L for these galaxies). Of the remaining galaxies none were detected ($>2\sigma$) in the epochs individually or combined (to [3.6] > 26.9, 2σ total).

3. STACKING

Owing to the extreme faintness of the z_{850}-dropout and Y_{105}-dropout samples over the WFC3 HUDF09 field, we derive average properties by registering and stacking the confusion corrected IRAC maps. The resulting stacked image for the 12 z_{850}-dropouts is shown in Figure 1, featuring an unambiguous source coincident with the z_{850}-dropout location, with an average magnitude of [3.6] = 27.2 (AB, measured in a $2\farcs5$ diameter aperture and corrected to total). To evaluate robustness of the detection we also create a median stack, which is resistant against outliers, to ensure that the signal is not coming from only a few sources. We derive uncertainties by bootstrap resampling the images in the stack 200 times, finding a signal-to-noise ratio (S/N) ≈ 5.1. The implied 1σ rms in a $2\farcs5$ aperture is [3.6] = 29.0 (total). The same procedure was carried out in the [4.5] band showing a fainter source (S/N = 2.6).

Detecting the Y_{105}-dropouts is even more challenging. Not only are the Y_{105}-dropouts in our samples fainter, there are also fewer to stack (4 versus 12), and they might be bluer due to younger ages, lower metallicities, or other effects (e.g., Bouwens et al. 2009b). The resulting stacked image for the 4 is shown in the lower panels of Figure 1, showing no detection to a limit [3.6] > 27.5 (2σ, total). The formal measurement is S/N = 0.9. The photometry is presented in Table 1.

The average SED shape of the faint $z \sim 7$ z_{850}-dropout galaxies, shown in Figure 2, is remarkably similar to that of the more luminous and massive NICMOS sample presented by Gonzalez et al. (2009). The rest-frame far-UV slope is extremely blue (Bouwens et al. 2009b find $\beta = -3.0 \pm 0.2$), suggesting low ages or sub-solar metallicities. However, note the relatively red $H_{160}-[3.6] = 0.7^{+0.2}_{-0.25}$ color, suggesting the presence of a modest Balmer break between the bands, indicative of evolved stellar populations.

4. STELLAR POPULATIONS

We use standard techniques to derive stellar masses and redshifts by fitting stellar populations synthesis models to the

[10] This paper uses data release DR3 of epoch 1 and data release DR2 of epoch 2, available from http://data.spitzer.caltech.edu/popular/goods/

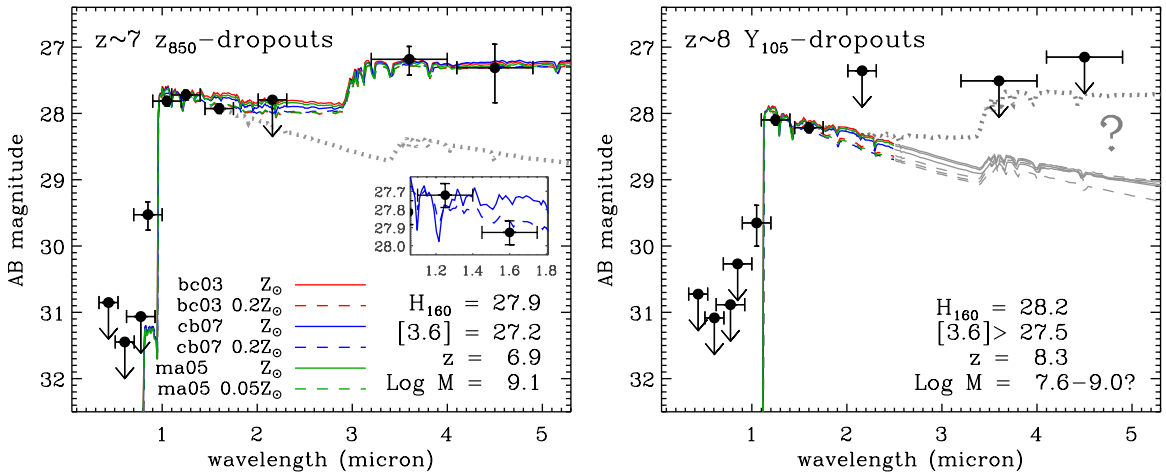

Figure 2. Average broadband ACS, WFC3/IR, and IRAC SEDs of the $z \sim 7$ and $z \sim 8$ galaxies. The left panel shows the average $z \sim 7$ z_{850}-dropout SED and the best-fit stellar population models. The blue far-UV slope and red $H_{160} - [3.6]$ color indicates a modest Balmer break, expected for evolved stellar populations (>100 Myr). Excluding the IRAC measurements leads to 1.5 dex smaller mass (dotted line). These faint galaxies have similar M/L and age as the luminous $z \sim 7$ sources presented by Gonzalez et al. (2009). The inset presents part of the SED around 1.4 μm (~1700 Å rest-frame) showing that the best-fit sub-solar metallicity models reproduce the quite blue far-UV slope better than do the best-fit solar models (see, e.g., Bouwens et al. 2009b for more details). Differences between the best-fit parameters of various stellar population models at fixed metallicity are small. The Y_{105}-dropouts (right panel) are undetected at [3.6]. The fit relies on the far-UV resulting in uncertain ages and masses. The gray dotted line shows the maximum M/L allowed by the fit (95% confidence). Clearly, moderately deeper IRAC would put stronger constraints on the allowed models at $z = 8$. Upper limits are 2σ. Note, the models were fitted to the fluxes of the $z \sim 7$ and $z \sim 8$ galaxies, not the upper limits.

(A color version of this figure is available in the online journal.)

Table 1
Stacked Photometry of $z \sim 7$ and $z \sim 8$ Dropout Galaxies in the HUDF

	B_{435}	V_{606}	i_{775}	z_{850}	Y_{105}	J_{125}	H_{160}	K_s	[3.6]	[4.5]
z_{850}-dropout SED	1.4(0.7)	0.4(0.4)	−0.1(0.6)	5.6(1.1)	27.2(1.8)	29.6(2.0)	24.5(1.6)	22.9(13.8)	48.5(9.5)	43.2(16.6)
Y_{105}-dropout SED	−1.1(0.9)	0.2(0.7)	0.3(0.8)	−0.8(1.4)	5.0(1.4)	20.9(1.4)	18.8(1.3)	15.1(20.7)	16.9(18.3)	20.5(25.0)

Notes. The optical-to-near-IR photometry is measured in 0.″4 diameter apertures and corrected to total. *Spitzer*/IRAC photometry is performed on confusion corrected maps in 2.″5 diameter apertures and corrected to total. Note, we limit the S/N to ≈ 15 or 0.07 mag to account for zero-point uncertainties. Units are nanoJy.

average i, z, Y, J, H, K, 3.6, 4.5-band flux densities of the z_{850}-dropouts and Y_{105}-dropouts. We use Bruzual & Charlot (2003, BC03) models and assume solar metallicity and a Salpeter (1955) initial mass function (IMF) between 0.1 and 100 $M_\odot$. This choice enables straightforward comparison with previous results, but we also review the effect of different assumptions and models. Furthermore, we assume constant star formation (CSF) as opposed to exponentially declining models, motivated by the lack of evolution of the star formation rate (SFR) per unit mass (specific SFR (SSFR)) between $z = 3$ and 7 (Gonzalez et al. 2009; Stark et al. 2009). Up to $A_V = 0.5$ mag Calzetti et al. (2000) starburst reddening is allowed, where we note that $z \gtrsim 5$ galaxies have blue UV-continuum slopes and low dust extinction (e.g., Lehnert & Bremer 2003; Stanway et al. 2005; Bouwens et al. 2006, 2009b). We use the χ^2-fitting code FAST (Kriek et al. 2009) which provides best-fit parameters and uncertainties using Monte Carlo simulations. We fit the average SED fluxes to models smoothed to a resolution of 100 Å rest frame, corresponding to the approximate width of the dropout selection windows. The modeling results are presented in Table 2 and overplotted in Figure 2.

The best-fit redshifts of the z_{850}-dropouts and Y_{105}-dropouts are $z = 6.9^{+0.1}_{0.1}$ and $z = 8.3^{+0.1}_{-0.2}$, respectively, in agreement with expectations from simulations (see Oesch et al. 2009b; Bouwens et al. 2009a). The extremely blue rest-frame far-UV slope of the $z \sim 7$ galaxies is a challenge to fit, requiring $A_V = 0$, and sub-solar metallicity rather than solar models ($\chi^2_{\rm red} = 2.9$ versus $\chi^2_{\rm red} = 6.4$). Consistently, the relatively red $(U - V)_{\rm rest} \approx 0.4$ color favors evolved models (age$_w$ $= 350^{+30}_{-170}$ Myr[11]). We caution that emission lines can contribute to the [3.6] flux, but for the redshift distribution and $H_{160} - [3.6]$ color of this sample we estimate the effect is only ~0.05–0.1 mag.

Interestingly, Maraston (2005) and S. Charlot & G. Bruzual (2010, in preparation; CB07) models produce nearly identical results as the BC03 models. Derived stellar masses are quite robust with at most 0.1 dex systematic variation between the different model choices. The only important effect on the masses is IMF: a more reasonable Kroupa (2001) IMF reduces the stellar masses and SFRs by 0.2 dex, but does not change other parameters or the quality of fit. More detailed exploration of the stellar ages and star formation histories (SFHs) is presented by Gonzalez et al. (2009).

The stellar masses and ages of the Y_{105}-dropout galaxies are not well constrained. The low S/N of the IRAC stack causes the fit to be determined by the J_{125} and H_{160} fluxes, producing a formal best fit with minimal allowed masses ~4×10^7 $M_\odot$ and ages ~10 Myr and ~1.5 dex uncertainties. However, if we refit the $z \sim 7$ stack without IRAC data we also find very low masses and ages and large uncertainties. This underscores the crucial importance of deep IRAC data and suggests that model fits relying exclusively on far-UV data should be regarded with

[11] Following Labbé et al. (2006) and Gonzalez et al. (2009), we report SFH weighted age$_w$ $= t/2$ (for CSF), where t is the time elapsed since the start of star formation.

Table 2
Best-fit Stellar Population Parameters for Constant Star-forming Models and a Salpeter (1955) IMF

Model	$z_{\rm phot}$	Z ($Z_\odot$)	log age$_w$ (yr)	A_V (mag)	log M^* ($M_\odot$)	log SFR ($M_\odot$ yr^{-1})	log SSFR (yr^{-1})	$\chi^2_{\rm red}$
z_{850}-dropouts solar metallicity								
BC03	$6.85^{+0.08}_{-0.07}$	1.00	$8.58^{+0.00}_{-0.28}$	$0.00^{+0.08}_{-0.00}$	$9.15^{+0.07}_{-0.28}$	$0.37^{+0.07}_{-0.02}$	$-8.78^{+0.21}_{-0.00}$	6.39
CB07	$6.85^{+0.07}_{-0.07}$	1.00	$8.58^{+0.00}_{-0.30}$	$0.00^{+0.05}_{-0.00}$	$9.15^{+0.05}_{-0.30}$	$0.37^{+0.05}_{-0.02}$	$-8.78^{+0.24}_{-0.00}$	6.39
MA05	$6.87^{+0.07}_{-0.07}$	1.00	$8.45^{+0.13}_{-0.36}$	$0.00^{+0.08}_{-0.00}$	$9.10^{+0.16}_{-0.36}$	$0.43^{+0.08}_{-0.02}$	$-8.67^{+0.32}_{-0.12}$	5.48
z_{850}-dropouts sub-solar metallicity								
BC03	$6.88^{+0.07}_{-0.07}$	0.20	$8.58^{+0.00}_{-0.32}$	$0.00^{+0.10}_{-0.00}$	$9.09^{+0.07}_{-0.29}$	$0.31^{+0.12}_{-0.01}$	$-8.78^{+0.25}_{-0.00}$	2.95
CB07	$6.88^{+0.08}_{-0.07}$	0.20	$8.55^{+0.03}_{-0.30}$	$0.00^{+0.12}_{-0.00}$	$9.07^{+0.10}_{-0.29}$	$0.31^{+0.14}_{-0.01}$	$-8.76^{+0.23}_{-0.02}$	2.94
MA05	$6.88^{+0.08}_{-0.07}$	0.05	$8.55^{+0.03}_{-0.32}$	$0.00^{+0.12}_{-0.00}$	$9.07^{+0.10}_{-0.28}$	$0.31^{+0.15}_{-0.01}$	$-8.76^{+0.23}_{-0.02}$	2.72
Y_{105}-dropouts solar metallicity								
BC03	$8.21^{+0.13}_{-0.19}$	1.00	$6.70^{+1.77}_{-0.00}$	$0.00^{+0.38}_{-0.00}$	$7.57^{+1.47}_{-0.03}$	$0.58^{+0.36}_{-0.27}$	$-6.99^{+0.00}_{-1.70}$	2.31
CB07	$8.21^{+0.14}_{-0.20}$	1.00	$6.70^{+1.77}_{-0.00}$	$0.00^{+0.40}_{-0.00}$	$7.57^{+1.51}_{-0.03}$	$0.58^{+0.39}_{-0.27}$	$-6.99^{+0.00}_{-1.70}$	2.31
MA05	$8.23^{+0.15}_{-0.23}$	1.00	$6.70^{+1.80}_{-0.00}$	$0.00^{+0.45}_{-0.00}$	$7.57^{+1.55}_{-0.03}$	$0.59^{+0.44}_{-0.23}$	$-6.98^{+0.00}_{-1.74}$	2.20
Y_{105}-dropouts sub-solar metallicity								
BC03	$8.26^{+0.15}_{-0.26}$	0.20	$6.70^{+1.80}_{-0.00}$	$0.00^{+0.50}_{-0.00}$	$7.59^{+1.45}_{-0.02}$	$0.60^{+0.50}_{-0.36}$	$-6.99^{+0.00}_{-1.72}$	1.57
CB07	$8.26^{+0.14}_{-0.25}$	0.20	$6.70^{+1.77}_{-0.00}$	$0.00^{+0.50}_{-0.00}$	$7.59^{+1.43}_{-0.02}$	$0.60^{+0.49}_{-0.36}$	$-6.99^{+0.00}_{-1.69}$	1.57
MA05	$8.26^{+0.14}_{-0.25}$	0.05	$6.70^{+1.77}_{-0.00}$	$0.00^{+0.50}_{-0.00}$	$7.58^{+1.44}_{-0.02}$	$0.60^{+0.49}_{-0.36}$	$-6.99^{+0.00}_{-1.70}$	1.62

Notes. Best-fit parameters and 68% confidence intervals as computed with FAST (Kriek et al. 2009) for CSF models with a Salpeter (1955) IMF between 0.1–100 $M_\odot$. A Kroupa (2001) IMF would result in 0.20 dex lower stellar masses and SFRs, respectively, but other parameters would remain unchanged. The z_{850}-dropout model fits favor low metallicities and high ages. The Y_{105}-dropout model fits are uncertain: deeper IRAC is needed. Note, following Gonzalez et al. (2009) we report the SFH averaged age$_w$ $= t/2$ (for CSF), where t is the time elapsed since the start of star formation.

caution. Even though the fits may suggest a strong evolution of the stellar populations, we cannot exclude that galaxies at $z \sim 8$ have similar masses, ages, and M/Ls as faint $z \sim 7$ galaxies.

5. DISCUSSION

The reionization epoch represents the latest frontier of galaxy formation theory, which is now being probed to extreme depths with the amazingly efficient WFC3/IR camera aboard *HST*. Using the conservative z_{850}-dropout and Y_{105}-dropout samples of Oesch et al. (2009b) and Bouwens et al. (2009a) we find *Spitzer*/IRAC capable of an equally remarkable feat: the stacked 3.6 μm detection of even the faintest $z \approx 6.9$ galaxies found by WFC3/IR, providing direct proof that IRAC can probe much deeper than widely accepted. In addition we derive upper limits for the newly discovered $z \approx 8.3$ galaxies, some of which may well be at higher redshift than the currently most distant $z \approx 8.2 \pm 0.1$ GRB (Salvaterra et al. 2009; Tanvir et al. 2009). We now elaborate on various implications.

1. *Stellar populations at $z \sim 7$.* *Spitzer*/IRAC places two important constraints on the stellar populations. First, the combination of the blue far-UV slope and the moderately red $H_{160}-[3.6] = 0.7^{+0.2}_{-0.25}$ color in the ultrafaint ($H_{160} \approx 27.9$) $z \sim 7$ galaxies indicates the presence of a modest Balmer break, expected for evolved stellar populations. Very young stellar ages are ruled out (CSF age$_w$ $\gtrsim$ 80 Myr at 95%). Interestingly, low-metallicity models, which produce bluer far-UV colors at fixed age, provide significantly better fits than do solar, but for both it is challenging to reproduce the extremely blue observed far-UV slope ($\beta = -3.0 \pm 0.2$ as found by Bouwens et al. 2009b). Second, the average stellar masses $\langle M \rangle \sim 1 \times 10^9\ M_\odot$ indicate appreciable mass-to-light ratios $M/L_{1500} \approx 0.1$ and $M/L_V \approx 0.2$. The ratios are comparable those of the more massive $\sim 7 \times 10^9\ M_\odot$ sample of Gonzalez et al. (2009), suggesting that the M/L ratios do not strongly depend on luminosity or mass. We find no appreciable difference between the best-fit parameters of BC03, MA05, and CB07 models, although IMF variations are a potentially significant source of systematic uncertainty: a steeper high-mass slope (e.g., Weidner & Kroupa 2005) would lower the inferred stellar ages, a higher characteristic mass (e.g., "bottom light," van Dokkum 2008) would lower the total stellar masses and M/Ls, and any evolution with time would complicate comparisons between SFR and stellar mass across epochs.
2. *Star formation histories.* SFHs are notoriously hard to constrain from observations of individual galaxies. However, statistical constraints can be obtained by comparing the SSFRs as a function of time and mass, as different shapes of the SFH give rise to distinctly different evolution (e.g., Labbé et al. 2007). One remarkable recent result is the observation that the SSFR at fixed $\sim 5 \times 10^9\ M_\odot$ does not evolve from $z = 3$–7 (Stark et al. 2009; Gonzalez et al. 2009). Here we benefit from the extreme depths of the WFC3/IR data to probe the lowest luminosities, suggesting that the SSFR at $z \sim 7$ is also not strongly dependent on luminosity or stellar mass over the range 1–7 $\times 10^9\ M_\odot$. This may imply that the SFR correlates with stellar mass with a logarithmic slope close to 1. Both results (with redshift and mass) qualitatively agree with numerical simulations for early galactic star formation ($z > 4$), which robustly predict that SFR is proportional to M*, with similar SFHs in haloes of different masses (Davé 2008), and that the SFRs of individual galaxies are constantly rising (Finlator et al. 2007).
3. *Evolution of the stellar mass density to $z = 7$–8.* The low-luminosity galaxies probed in this paper are expected to contribute significantly to the stellar mass density owing to their substantial M/L. Following the approach of Gonzalez

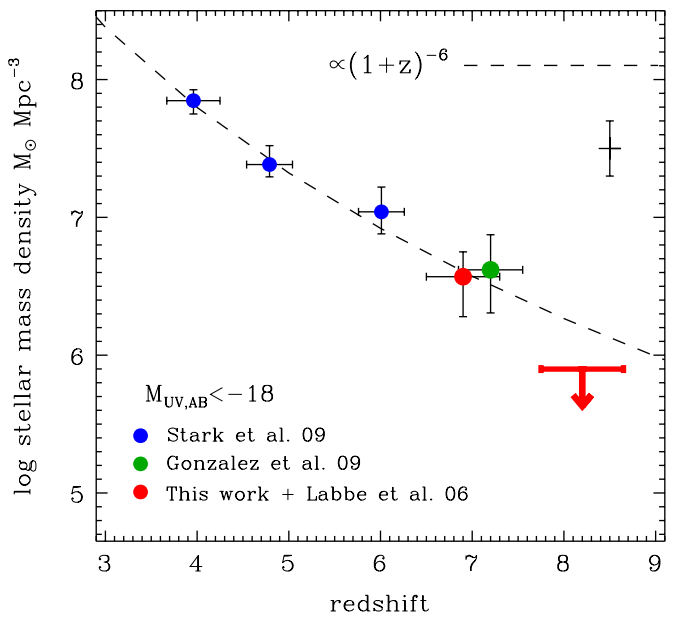

Figure 3. Evolution of the integrated stellar mass density. The red circle shows the $z \sim 7$ mass density, derived by multiplying the integrated UV-luminosity density of Bouwens et al. (2009a) with the mean M/L of the sample studied here. The other $z = 3$–7 results are based on luminous samples ($M_{UV,AB} < -20$) from the literature (e.g., Stark et al. 2009, blue circles; Gonzalez et al. (2009), green circle), corrected by +0.75 dex to $M_{UV,AB} < -18$, as appropriate for the UV LF of Bouwens et al. (2008) and a constant M/L. The dashed line shows a $\propto (1+z)^{-6}$ evolution. The $z = 8$ upper limit shows the 95% confidence interval on the M/L, which is marginally in agreement with the extrapolated evolution. The floating error bar indicates the expected cosmic variance for the $z \sim 7$ and $z \sim 8$ samples.

(A color version of this figure is available in the online journal.)

et al. (2009), we derive integrated stellar mass densities at $z = 7$–8 by multiplying the UV-luminosity densities of Bouwens et al. (2009a), integrated to $M_{UV,AB} = -18$, with the mean M/L derived for the galaxy samples in this Letter. For the z_{850}-dropouts at $z \sim 7$, this results in $\rho^* = 3.7^{+1.4}_{-1.8} \times 10^6\ M_\odot$ Mpc^{-3}. The evolution of the mass density is shown in Figure 3, compared to previous luminous samples, which were corrected to the same luminosity limit assuming a constant M/L. The stellar masses at $z = 8$ are uncertain by ~1.5 dex due to the weak constraints from IRAC, so instead of plotting the best-fit M/L we show the 95% confidence upper limit. The integrated mass density to a limit of $M_{UV,AB} < -18$ then declines to $<8 \times 10^5\ M_\odot$ Mpc^{-3}. This is marginally consistent with the extrapolation of the $\propto (1+z)^{-6}$ evolution over the range $3 < z < 7$. The upper limit may be evidence for a more rapid evolution toward $z = 8$, but deeper IRAC data and larger samples are needed to establish this firmly. The uncertainties quoted above do not include cosmic variance, which is estimated to be ~30% for the $z \sim 7$ sample and ~40% at $z \sim 8$ (Trenti & Stiavelli 2008).

4. *Reinionization since* $z \sim 11$. Combined, the results have profound implications for the ability of the universe to be reionized by photons from star formation—and to remain so for an extended period. Crucially, the large stellar mass density in $z \sim 7$ low-luminosity galaxies points to significant amounts of star formation at earlier times. We can therefore ask whether this corresponds to enough ionizing photons at higher redshift to keep the universe reionized. Let us assume the stellar mass density $\rho^* = 3.7 \times 10^6\ M_\odot$ Mpc^{-3} was assembled in the 340 Myr between $7 < z < 11$, in the reionization era (*WMAP5*; Komatsu et al. 2009). Correcting by 10% to account for mass loss in stellar evolution, the possible sustained SFR density would then be $\rho_{SFR} \approx 0.012\ M_\odot$ yr^{-1} Mpc^{-3}, significantly higher than that has been derived for luminous galaxies alone (Gonzalez et al. 2009). However, the primary uncertainty is the fiducial critical SFR density needed for reionization $\rho^{SFR}_{crit} \propto C/f_{esc}$ (Madau et al. 1999), which depends sensitively on the values for the H II IGM clumping factor $1 < C < 30$ and the fraction of ionizing photons $0.05 < f_{esc} < 1$ that leak unhindered out of the galaxies (e.g., Ouchi et al. 2009). The popular choice ($C = 30$, $f_{esc} = 0.1$) leads to $\langle \rho^{SFR}_{crit} \rangle = 0.7\ M_\odot$ yr^{-1} Mpc^{-3} averaged over $7 < z < 11$, which is 60 times higher than that can be explained by the stellar masses. However, at early times the clumping factor may be as low as $C = 3$–6 (e.g., Trac & Cen 2007; Bolton & Haehnelt 2007; Pawlik et al. 2009). The escape fraction may be significantly higher as well: recent numerical simulations suggest $f_{esc} \gtrsim 0.2$ (Wise & Cen 2009; Pawlik et al. 2009; Yajima et al. 2009) and Bouwens et al. (2009b) note that the extremely blue far-UV slope of the galaxies studied here could also result from large escape fractions $f_{esc} \gtrsim 0.3$. The choice ($C = 3$, $f_{esc} = 0.5$) leads to $\langle \rho^{SFR}_{crit} \rangle \approx 0.014\ M_\odot$ yr^{-1} Mpc^{-3}(over $7 < z < 11$), which means photons from the low-luminosity star-forming galaxies observed here are capable of causing sustained reionization since $z = 11$.

The first *Spitzer*/IRAC detection of low-luminosity $z = 7$ galaxies and their red $H - [3.6] \approx 0.7$ colors provide important insights into the earliest phases of galaxy evolution, showing that these early galaxies have relatively high ~300 Myr ages and $M/L_V \approx 0.2$. Consequently, low-luminosity galaxies contribute significantly to the stellar mass density $\rho^*(z = 7) = 3.7^{+1.4}_{-1.8} \times 10^6\ M_\odot$ Mpc^{-3}, suggesting that the SFR corresponding to that mass may have provided a substantial fraction of the ionizing photons that kept the universe reionized at earlier times. Future IRAC studies of larger numbers of high-redshift galaxies are required to bolster the results in this paper and to further constrain the evolution of the mass density toward the highest redshifts $z \gtrsim 8$. The *Spitzer* post-cryogenic phase ("warm mission") provides a rare window of opportunity to observe these galaxies in a timely manner to the ~0.5 mag deeper limits needed, long before the arrival of the *James Webb Space Telescope* (*JWST*).

We are grateful to all those at NASA, STScI, JPL, SSC, and throughout the community who have worked so diligently to make *Hubble* and *Spitzer* the remarkable observatories that they are today. We thank Kristian Finlator, Masami Ouchi, and Risa Wechsler for stimulating discussion. I.L. acknowledges support from NASA through Hubble Fellowship grant HF-01209.01-A awarded by the STScI, which is operated by the AURA, Inc., for NASA, under contract NAS 5-26555. P.O. acknowledges support from the Swiss National Foundation (SNF). We acknowledge the support of NASA grant NAG5-7697 and NASA grant HST-GO-11563.01.

Facilities: Spitzer (IRAC), *HST* (WFC3/IR), *Magellan:* Baade (PANIC), VLT: Melipal (ISAAC)

REFERENCES

Bolton, J. S., & Haehnelt, M. G. 2007, MNRAS, 374, 493
Bouwens, R. J., Illingworth, G. D., Blakeslee, J. P., & Franx, M. 2006, ApJ, 653, 53

Bouwens, R. J., Illingworth, G. D., Franx, M., & Ford, H. 2008, ApJ, 686, 230
Bouwens, R. J., et al. 2009a, arXiv:0909.1803
Bouwens, R. J., et al. 200b, ApJ, in press (arXiv:0910.0001)
Bunker, A., et al. 2009, arXiv:0909.2255
Bruzual, G., & Charlot, S. 2003, MNRAS, 344, 1000 (BC03)
Calzetti, D., et al. 2000, ApJ, 533, 682
Castellano, M., et al. 2009, arXiv:0909.2853
Davé, R. 2008, MNRAS, 385, 147
Eyles, L. P., et al. 2005, MNRAS, 364, 443
Egami, E., et al. 2005, ApJ, 618, L5
Fazio, G. G., et al. 2004, ApJS, 154, 10
Finlator, K., Davé, R., & Oppenheimer, B. D. 2007, MNRAS, 376, 1861
Gonzalez, V., Labbe, I., Bouwens, R. J., Illingworth, G., Franx, M., Kriek, M., & Brammer, G. B. 2009, arXiv:0909.3517
Kriek, M., van Dokkum, P. G., Labbé, I., Franx, M., Illingworth, G. D., Marchesini, D., & Quadri, R. F. 2009, ApJ, 700, 221
Kroupa, P. 2001, MNRAS, 322, 231
Komatsu, E., et al. 2009, ApJS, 180, 330
Labbé, I., Bouwens, R., Illingworth, G. D., & Franx, M. 2006, ApJ, 649, L67
Labbé, I., et al. 2003, AJ, 125, 1107
Labbé, I., et al. 2007, ApJ, 665, 94
Lehnert, M. D., & Bremer, M. 2003, ApJ, 593, 630
Madau, P., Haardt, F., & Rees, M. J. 1999, ApJ, 514, 648
Maraston, C. 2005, MNRAS, 362, 799
McLure, R. J., Cirasuolo, M., Dunlop, J. S., & Foucaud, S. 2009a, MNRAS, 395, 2196
McLure, R. J., Dunlop, J. S., Cirasuolo, M., Koekemoer, A. M., Sabbi, E., Stark, D. P., Targett, T. A., & Ellis, R. S. 2009b, MNRAS, in press (arXiv:0909.2437)
Oesch, P. A., et al. 2009a, ApJ, 690, 1350
Oesch, P. A., et al. 2009b, ApJ, in press (arXiv:0909.1806)
Oke, J. B., & Gunn, J. E. 1983, ApJ, 266, 713
Ouchi, M., et al. 2009, ApJ, 706, 1136
Pawlik, A. H., Schaye, J., & van Scherpenzeel, E. 2009, MNRAS, 394, 1812
Salpeter, E. E. 1955, ApJ, 121, 161
Salvaterra, R., et al. 2009, Nature, 461, 1258
Stanway, E. R., Bunker, A. J., & McMahon, R. G. 2003, MNRAS, 342, 439
Stanway, E. R., McMahon, R. G., & Bunker, A. J. 2005, MNRAS, 359, 1184
Stark, D. P., Ellis, R. S., Bunker, A., Bundy, K., Targett, T., Benson, A., & Lacy, M. 2009, ApJ, 697, 1493
Stark, D. P., Ellis, R. S., Richard, J., Kneib, J.-P., Smith, G. P., & Santos, M. R. 2007, ApJ, 663, 10
Tanvir, N. R., et al. 2009, Nature, 461, 1254
Trenti, M., & Stiavelli, M. 2008, ApJ, 676, 767
Trac, H., & Cen, R. 2007, ApJ, 671, 1
Yajima, H., Umemura, M., Mori, M., & Nakamoto, T. 2009, MNRAS, 398, 715
Yan, H., Dickinson, M., Giavalisco, M., Stern, D., Eisenhardt, P. R. M., & Ferguson, H. C. 2006, ApJ, 651, 24
Yan, H., et al. 2004, ApJ, 616, 63
van Dokkum, P. G. 2008, ApJ, 674, 29
Weidner, C., & Kroupa, P. 2005, ApJ, 625, 754
Wise, J. H., & Cen, R. 2009, ApJ, 693, 984
Wuyts, S., et al. 2007, ApJ, 655, 51